EasyChair Preprint

№ 2481

Performance Analysis of Grid Connected SPV Inverter for FLC and ANFIS Based Controller

Ranjit Singh, Sumit Kataria and Pushkar Kumar

January 29, 2020

Performance Analysis of Grid Connected SPV Inverter for FLC and ANFIS Based Controller

Ranjit Singh[1], Sumit Kataria[2], Pushkar Kumar[3]

[1] Assistant Professor, Electrical Engg. department, Quantum school of technology, Quantum University, Roorkee, Utrakahand
ranjit.ee@quantumeducation.in
[2] Assistant Professor, Electrical Engg. department, Quantum school of technology, Quantum University, Roorkee, Utrakahand
sumitkataria.ee@quantumeducation.in
[3] Assistant Professor, Electrical Engg. department, Quantum school of technology, Quantum University, Roorkee, Utrakahand
pushkarkumar.ee@quantumeducation.in

Abstract. Maximum Power Point Tracking (MPPT) is used in Solar Photovoltaic (SPV) systems to maximize the photovoltaic array output power, irrespective of the temperature and irradiation conditions and of the load electrical characteristics. This paper proposes a mathematical model for three-phase SPV systems with MPPT control. The parametric equation of SPV cell, MPPT algorithm for tracking maximum power from the PV source, integration of PV model with the grid through a DC-DC boost converter and a three-phase PWM inverter are discussed. The detailed model is developed to perform the comparison of different controller in terms of switching losses, junction temperature and sink temperature of power electronics devices. The resulting system has high efficiency, lower cost and can be easily modified for different applications. Fuzzy logic control (FLC) method and Adaptive neuro fuzzy inference (ANFIS) based controller is used for MPPT, giving the basis for reference current generation and in turn effectively control the PWM inverter feeding power to the grid. The performance evaluation has been carried out for duty cycle of DC-DC boost converter for both controller for various outputs of the SPV array, in terms of energy injected to grid, switching losses, junction temperature and sink temperature. The results validated the effectiveness of the MPPT algorithm in increasing SPV output energy, decrease in the switching losses, junction & sink temperature. The results show that ANFIS method is slightly better to FLC method in energy injected to the grid with lower switching losses, junction & sink temperature

Keywords: ANFIS, FLC, MPPT, SPV

1 Introduction

Renewable energy plays an important role in electric power generation. Various renewable energy sources such as solar energy, wind energy, geothermal etc, are harness for electric power generation. Specially, solar energy has the advantage of no pollution, low maintenance cost, no installation area limitation, and no noise due to the absence of the moving parts. Because of non-linear relation between the current and the

voltage of the photovoltaic cell, it can be observed that there is unique Maximum Power Point (MPP) at a particular environment, and this peak power point keeps changing with solar illumination and ambient temperature. An important consideration in achieving high efficiency in Solar Photovoltaic (SPV) power generation is to match the SPV source and load impedance properly for any weather condition, thus obtaining maximum power generation [1]. In recent years, a large number of techniques have been proposed for Maximum Power Point Tracking (MPPT) such as fractional open circuit voltage, Fractional short circuit current, Perturb and Observe (P&O) method, Incremental Conductance (INC) method and some based on Computational Intelligence (CI) techniques such as Fuzzy logic (FLC), Artificial neural network (ANN), Genetic algorithm (GA). The non linear relationship between voltage at maximum power (V_{MPP}) and Open Circuit Voltage (V_{OC}) of the PV array, under varying irradiance and temperature levels, has given rise to the fractional V_{OC} method [2]-[9]. This method is very simple and less complex. Similarly Fractional short circuit current(I_{SC}) results from the fact that, under varying atmospheric conditions, current at maximum power(I_{MPP}) is approximately linearly related to the I_{SC} of the PV array [10]-[12]. Fuzzy logic controllers (FLC) have the advantages of working with imprecise inputs, not needing an accurate mathematical model, and handling nonlinearity [13]-[17]. Another intelligent technique is the adaptive neuro fuzzy inference system [18]-[21]. In order to improve efficiency and gain better quality of output power in SPV generation system, INC based MPPT algorithm for DC-DC boost converter based on FLC controller and ANFIS controller is compared in this paper. The scope of the work is to first give the detailed mathematical model of grid connected three-phase SPV system. A parametric model of SPV cell is presented. Second, thermal modelling & switching loss calculation of switching devices are discussed and then the performance evaluation has been carried out for FLC and ANFIS based MPPT algorithm for various operating conditions of the SPV array, in terms of energy injected to grid, switching losses, junction, case and sink temperatures, for switching in the DC-DC boost converter. The results validated the effectiveness of the MPPT algorithm in increasing SPV output energy, decrease in the switching losses, junction & sink temperature. The results show that ANFIS based controller is slightly better to FLC based controller in energy injected to the grid with lower switching losses, junction & sink temperature.

2 Mathematical model of three phase grid connected SPV system

2.1 Introduction

The power conversion topology adopted is given in Fig.1. Due to the mismatch of the minimum SPV field working voltage and the minimum DC-link voltage required from DC/AC output stage feeding the grid, an input DC/DC voltage boost converter is required. schematic diagram of grid connected SPV array system is thus composed of the SPV array, DC/DC Boost converter, DC/AC Inverter and grid, as illustrated in Fig.1.

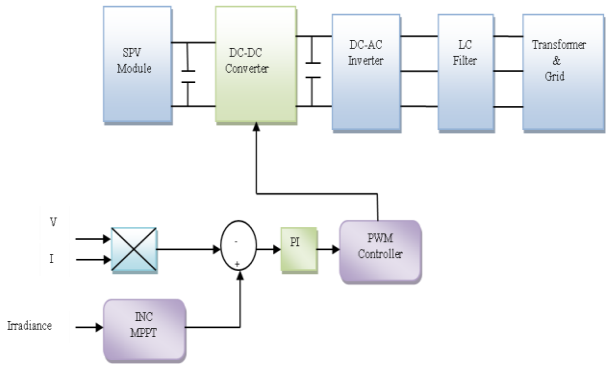

Fig. 1. Three phase grid connected spv system

2.2 Model of the SPV array

The equivalent circuit of the solar cell is given below in fig 2. I_{ph} is the cell photocurrent that is proportional to solar irradiation, I_{rs} is the cell reverse saturation current that mainly depends upon the temperature, K_o is a constant, N_s and N_p are the number of series and parallel strings in the PV array respectively. Generally, a PV module comprises of a number of PV cells connected in either series or parallel and its mathematical model can be simply expressed as below. Where I denotes the PV array output current, V is the PV output voltage, I_{ph} is the cell photocurrent that is proportional to solar irradiation, R_s and R_p is the series and parallel resistance of the PV array. The equation describing the I-V characteristics of the solar array are as follows [22]:

$$I = N_{ph} I_{ph} - N_p I_{rs} \left[\exp\left(K_0 \frac{V}{N_s} \right) - 1 \right] \tag{1}$$

where, I denotes the PV array output current, V is the PV array output voltage. All of the constants in the above equation can be determined by examining the manufacturer rating of the SPV array and then the published or measured I-V curves of the array as described in Table 1. As a typical case, the Sun Power modules (SPR-305) array is used to illustrate and verify the model. The model parameters are given in Table 1 and can be found in the datasheet [23].

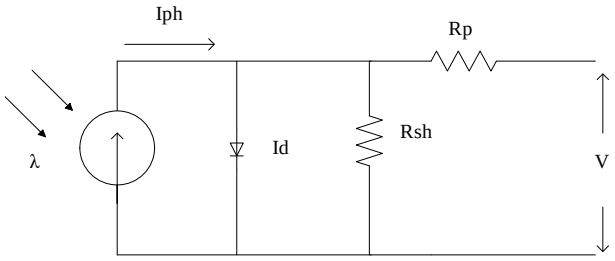

Fig. 2. Equivalent circuit of solar cell

As can be derived clearly from (1), the SPV array exhibits a highly nonlinear radiation and temperature dependent I-V and P-V characteristic curve, both curves being simulated at Sun Power modules (SPR-305) and illustrated in Fig.3.& Fig.4.

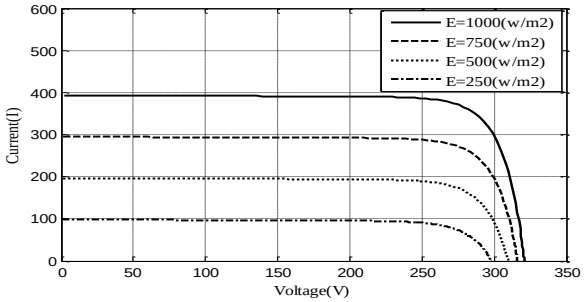

Fig. 3. Simulated i-v characteristics of sun power module(SPR-305) at irradiance g=1kW/m^2 valued at temp. 25^{0}C

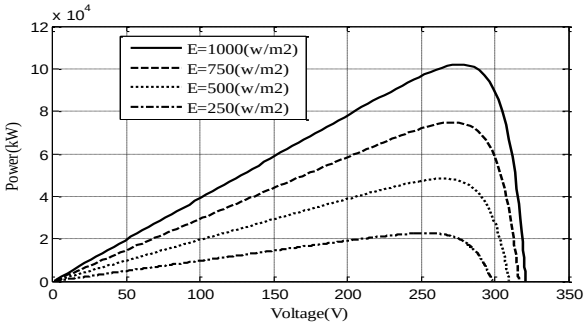

Fig. 4. Simulated p-v characteristics of sun power module(SPR-305) at irradiance g=1kW/m^2 valued at temp. 25^{0}C

2.3 Voltage boost converter & MPPT algorithm

For Maximum energy exploitation, it is reasonable to work at the MPP. The simplest form of DC-DC boost converter based on single switch and input inductor is used. The boost topology is capable of raising input voltage to the intermediate DC-link voltage, only limitation due to efficiency drop at very low voltage [24]. The boost converter equivalent circuit is shown in Fig. 5 depending on the load and the circuit parameters, the inductor current can be either continuous or discontinuous. The inductor value, L, required to operate the converter in continuous conduction mode is calculated such that the peak inductor current at maximum output power does not exceed the power switch current rating. Thus, L and output capacitor value, C, to give the desired peak-to-peak output ripple is calculated as:

$$L=\frac{(1-D)^2}{2f} \quad \text{and} \quad C \geq \frac{DV_0}{V_r R f} \tag{2}$$

Where f is switching frequency, D is duty cycle of the IGBT switch, R is the load resistance, V_o is output voltage and V_r is peak-to-peak ripple voltage. The DC-DC boost converter has the following simplified input-output equation.

$$V_i = (1 - D)V_0 \tag{3}$$

Where V_o is the DC-link voltage regulated to be constant by the DC-link PI voltage control. So D is the degree of freedom to change the work point of the SPV cells.

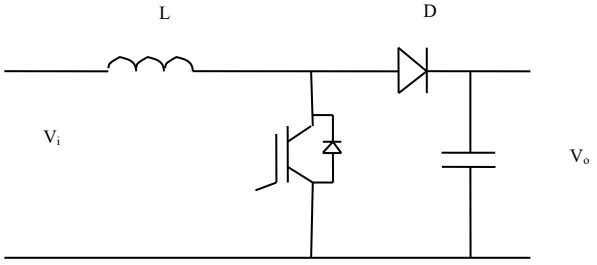

Fig. 5. DC-DC boost converter

The PV output power is used to directly control the power converter duty cycle to reduce well the complexity of the system. In order to overcome the limitations of conventional control techniques for the complex SPV systems, an FLC [25] has been utilized. The FLC has been trained with the input and output data obtained from the transient simulations of the conventional (PI) controller with different operating conditions. The FLC acts like the conventional (PI) controller without the need to

design and tuned for different operating conditions. The basic concepts of fuzzy and FLC are briefly presented in following sub-sections.

2.4 Fuzzy Logic

The fuzzy logic basically maps an input space to an output space, primarily through a list of if-then statements, called rules. All rules are evaluated in parallel, and however, the order of the rules is not important. The rules, themselves, are useful, because they refer to the variables and the adjectives that describe those variables. Before building a system that interprets the rules, the terms to be used and the adjectives, that describe them, have to be defined. The basic block diagram of a fuzzy logic system is shown in Fig.6. As depicted in Fig.6, a fuzzy inference is a method that interprets the values in the input vector and assigns values to the output vector based on set of rules. The fuzzy inference system maps crisp set of input variables into a fuzzy set by using membership functions and based on these fuzzy input sets, according to the predefined logic, the output is assigned.

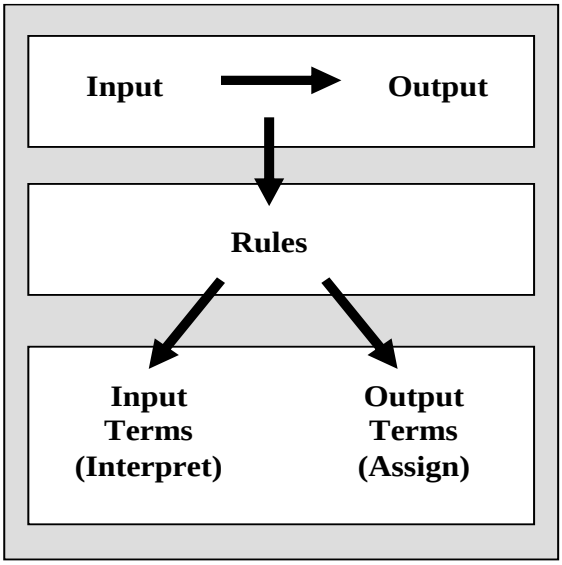

Fig.6. Basic block diagram of fuzzy logic system

Some Important Terms Used in Fuzzy Logic
Fuzzy Set is a set without a crisp, which clearly defines boundary. It can contain elements with only a partial degree of membership.
Membership Function (MF) is a curve that defines how each point in the input space is mapped to a membership value (or degree of membership) between 0 and 1. The input space is sometimes referred to as the universe of discourse. The only condition, a membership function must really satisfy, is that it must vary between 0 and 1.The

function itself can be an arbitrary curve whose shape can be defined as a function that suits from the point of view of simplicity, convenience, speed, and efficiency.

Fuzzy Logic Operators: There are three kinds of logical operators in the fuzzy logic; fuzzy intersection or conjunction (AND), fuzzy union or disjunction (OR), and fuzzy complement (NOT). The AND operation is carried out by using min (minimum) function, OR operation is carried out by max (maximum) function and NOT by complement function. Fig. 7 shows an example of the fuzzy logic operators. Suppose there are two statements A and B, AND, OR and NOT operation on these statements are shown in this figure. Even though the example is shown for binary values 1 and 0, the logical operators can also be applied to the statements having value other than binary, lying between 1 and 0.

AND

A	B	Min(A,B)
0	0	0
0	1	0
1	0	0

OR

A	B	Max(A,B)
0	0	0
0	1	1
1	0	1

NOT

A	1-A
0	1
1	0

Fig.7. Examples of fuzzy logic operators

The intersection of two fuzzy sets A and B is specified, in general, by a binary mapping T, which aggregates two membership functions as follows:

$\mu A \cap B(x) = T(\mu A(x), \mu B(x))$

For example, the binary operator T may represent the multiplication of membership functions $\mu A(x)$ and $\mu B(x)$. These fuzzy intersection operators, which are usually

referred to as T-norm (Triangular norm) operators, meet the following basic requirements.
A T-
norm operator is a binary mapping T(.,.) satisfyingboundary: T(0, 0) = 0, T(a, 1) = T(1, a) = a
monotonicity: T(a, b) $\leq$ T(c, d) if a $\leq$ c and b $\leq$ d
commutativity: T(a, b) = T(b, a)
associativity: T(a, T(b, c)) = T(T(a, b), c)
The first requirement imposes the correct generalization to crisp sets. The second requirement implies that a decrease in the membership values in A or B cannot produce an increase in the membership value in A intersection B. The third requirement indicates that the operator is indifferent to the order of the fuzzy sets to be combined. Finally, the fourth requirement allows us to take the intersection of any number of sets in any order of pairwise groupings.
Like fuzzy intersection, the fuzzy union operator is specified, in general, by a binary mapping S
$\mu A \cup B(x) = S(\mu A(x), \mu B(x))$
For example, the binary operator S can represent the addition of membership functions $\mu A(x)$ and $\mu B(x)$. These fuzzy union operators, which are often referred to as T-conorm (or S-norm) operators, must satisfy the following basic requirements.
A Tconorm (or Snorm) operator is a binary mapping S(.,.) satisfying
boundary: S(1, 1) = 1, S(a, 0) = S(0, a) = a
monotonicity: S(a, b) $\leq$ S(c, d) if a $\leq$ and b $\leq$ d
commutativity: S(a, b) = S(b, a)
associativity: S(a, S(b, c)) = S(S(a, b), c)
Fuzzy Rules (If-Then Rules): Fuzzy sets and fuzzy operators are the subjects and verbs of fuzzy logic. These 'if-then rules' statements are used to formulate the conditional statements that comprise fuzzy logic.
A single fuzzy if-then rule assumes the form "if x is A then y is B", where A and B are linguistic values defined by fuzzy sets on the ranges (universes of discourse) X and Y, respectively. The if-part of the rule "x is A" is called the antecedent or premise, while the then-part of the rule "y is B" is called the consequent or conclusion. Interpreting if-then rules is a three-part process.
Fuzzy Inference Systems
Fuzzy Inference Systems (FIS) are also known as fuzzy rule based systems, fuzzy models, fuzzy associative memories, or fuzzy controllers, when used as controllers. Fuzzy inference is the process of formulating the mapping from a given input to an output using fuzzy logic. The mapping, then, provides a basis from which decisions can be made. The process of fuzzy inference involves all of the processes that are described above.
Basically, a FIS consists of five functional blocks as shown in Fig. 8 [26].
A rule base, containing a number of fuzzy if-then rules.
A data base, which defines the membership functions of the fuzzy sets used in the fuzzy rules.
A decision- making unit, which performs the inference operations on the rules.
A fuzzification interface, which transforms the crisp inputs into linguistic values.

A defuzzification interface, which transforms the fuzzy results into a crisp output. Generally, the rule base and data base are jointly referred to as the knowledge base.There are two types of fuzzy inference systems Mamdani- type and Sugeno-type. These two types of inference systems vary, somewhat, in the way outputs are determined. Mamdani's fuzzy inference method is the most commonly used fuzzy methodology. Mamdani's method was among the first control systems built using fuzzy set theory. It was proposed in 1975 by Ebrahim Mamdani as an attempt to control a steam engine and boiler combination by synthesizing a set of linguistic control rules obtained from experienced human operators. Fig.9. shows all parts of the fuzzy inference process. Information flows through the fuzzy inference diagram as shown below. The flow proceeds up from the inputs in the lower left, then across each row, or rule, and then down the rule outputs to finish in the lower right. This is a very compact way of showing everything at one place, from linguistic variable fuzzification all the way through defuzzification of the aggregate output.

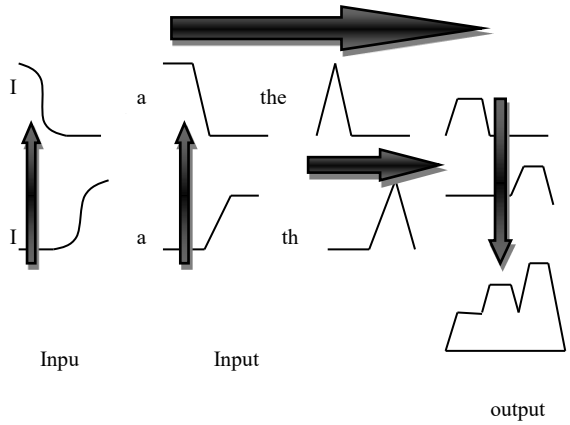

Fig.9. Fuzzy inference system

2.5 Adaptive neuro fuzzy inference system based controller

The basic structure of fuzzy inference system seen, so far, is a model that maps input characteristics to input membership functions, input membership function to rules, rules to a set of output characteristics, output characteristics to output membership functions, and the output membership function to a single-valued output or a decision associated with the output. In both Mamdani and Sugeno type of inference systems, when used for data modeling, membership functions and rule structure are essentially predetermined by the human interpretation of the characteristics of the variables of the data model. The shape of the membership functions depends on the values of the parameters. Instead of just looking at the data to choose the membership function parameters, by using ANFIS membership function, the parameters can be chosen automatically. The basic idea behind neuro-adaptive learning techniques is very simple. These techniques provide a method for the fuzzy modeling procedure to learn information about a data

set, in order to compute the membership function parameters that best allow the associated fuzzy inference system to track the given input/output data. This learning method works similar to the neural networks. In an adaptive neuro-fuzzy inference technique, using a given input/output data set, a fuzzy inference system (FIS) is constructed, whose membership function parameters are tuned (adjusted) using either a back-propagation algorithm alone, or in combination with a least squares type of method. This allows fuzzy systems to learn from the data. A network-type structure, similar to that of a neural network, which maps inputs through input membership functions and associated parameters, and then through output membership functions and associated parameters to outputs, can be used to interpret the input/output map. Fig.10. shows the basic structure of the ANFIS algorithm for a first order Sugeno-type fuzzy system. The various layers shown in Fig.10. are explained below [26].

Layer1

Every node i, in this layer, is a square node with a node function

$$O_i^1 = \mu_{A_i}(x)$$

where, x is the input to node i, and Ai is the linguistic label (small, large, etc.,) associated with this node function. In other words, oi1 is the membership function of Ai and it specifies the degree to which the given x satisfies the quantifier Ai. Usually μAi(x) is selected to be bell shaped with maximum value equal to 1, and minimum value equal to 0, such as

$$\mu_{A_i}(x) = \frac{1}{1+\left[\left(\frac{x-c_i}{a_i}\right)^2\right]^{b_i}}$$

or

$$\mu_{A_i}(x) = \exp\left\{-\left(\frac{x-c_i}{a_i}\right)^2\right\}$$

where, [34] is the parameter set. As the values of these parameters change, the bell-shaped functions vary accordingly, thus exhibiting various forms of membership functions on linguistic label Ai. In fact any piecewise differentiable function, such as commonly used trapezoidal or triangular-shaped membership function, is also qualified candidates for node functions in this layer. Parameters in this layer are referred to as premise parameters.

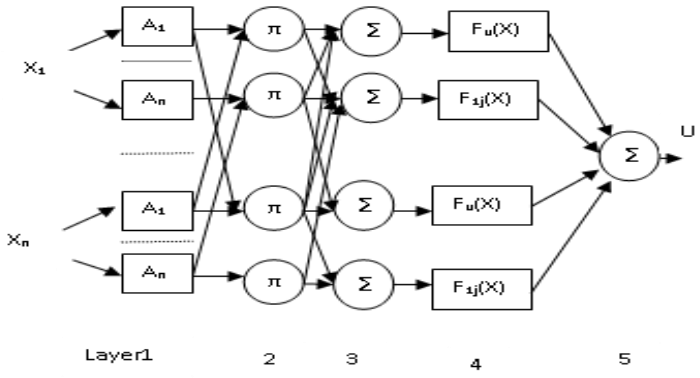

Fig.10. Typical ANFIS structure

Layer 2
Every node in this layer is a circle node, labeled Π, which multiplies the incoming signals and sends the product out. For example

$w_i = \mu_{A_i}(x)\, X\, \mu_{B_i}(y)$, i =1, 2.

Each node output represents the firing strength of a rule. In fact, other T-norm operators that performs generalized AND can be used as the node function in this layer.
Layer 3
Every node in this layer is a circle node, labeled N. The ith node calculates the ratio of the ith rule's firing strength to the sum of all rule's firing strengths, as given below.

$$\overline{w}_i = \frac{w_i}{w_1 + w_2}, i = 1, 2.$$

Outputs of this layer are known as normalized firing strengths.
Layer 4
Every node i in this layer is a square node with a node function

$$O_i^4 = \overline{w}_i\, f_i = \overline{w}_i (p_i x + q_i y + r_i)$$

where, $\overline{w}_i$ is the output of layer 3, and { p_i , q_i , r_i }is the parameter set. Parameters in this layer will be referred to as consequent parameters.
Layer 5
The single node in this layer is a circle node labeled Σ that computes overall output as the summation of all incoming signals, i.e,

$$O_i^5 =_i overall\, output = \sum_i \overline{w}_i\, f = \frac{\sum_i w_i f_i}{\sum_i w_i}$$

The adjustment of modifiable parameters is a two-step process. First, information are propagated forward in the network until Layer-4, where the parameters are identified by a least-squares estimator. Then, the parameters in Layer-2 are modified using gradient descent. The only user specified information is the number of membership

functions in the universe of discourse for each input and output as training information. ANFIS uses back propagation learning to learn the parameters related to membership functions and least mean square estimation to determine the consequent parameters. Every step in the learning procedure includes two parts. The input patterns are propagated, and the optimal consequent parameters are estimated by an iterative least mean square procedure. The premise parameters are assumed fixed for the current cycle through the training set. The pattern is propagated again, and in this epoch (iterations), back propagation is used to modify the premise parameters, while the consequent parameters remain fixed.The parameters associated with the membership functions will change through the learning process. The computation of these parameters (or their adjustment) is facilitated by a gradient vector, which provides a measure of how well the fuzzy inference system is modeling the input/output data for a given set of parameters. Once the gradient vector is obtained, some of the available optimization routines can be applied to adjust the parameters so as to reduce some error measure (usually defined by the sum of the squared difference between actual and desired outputs).

2.6 Design of fuzzy logic controller

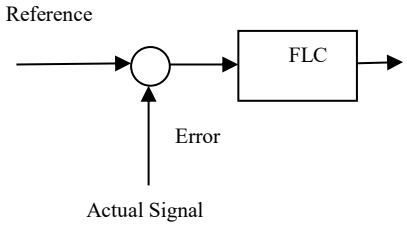

Fig.11. Design of fuzzy logic controller

The PI controllers are replaced by FLC and a typical control diagram is shown in Fig.11. Fuzzy Logic tool box in MATLAB has been used for designing and testing of the FLC.The data required for training and testing the FLC are generated by designing and testing PI controllers for a set of different solar irradiance conditions.The FLC has two input value E (k) and CE (k) in sampling time k.The fuzzy linguistic value defines seven step of positive big (PB), positive middle (PM), positive small (PS), zero (ZO), negative small (NS), negative middle (NM) and negative big (NB). Fig.12. shows fuzzy membership function according to seven basic linguistic value for input and output value[27].These membership function has been used due to simplicity as compared to another membership functions. The range of E, CE and DU has been decided according to the data obtained from the performance of the conventional PI controller.

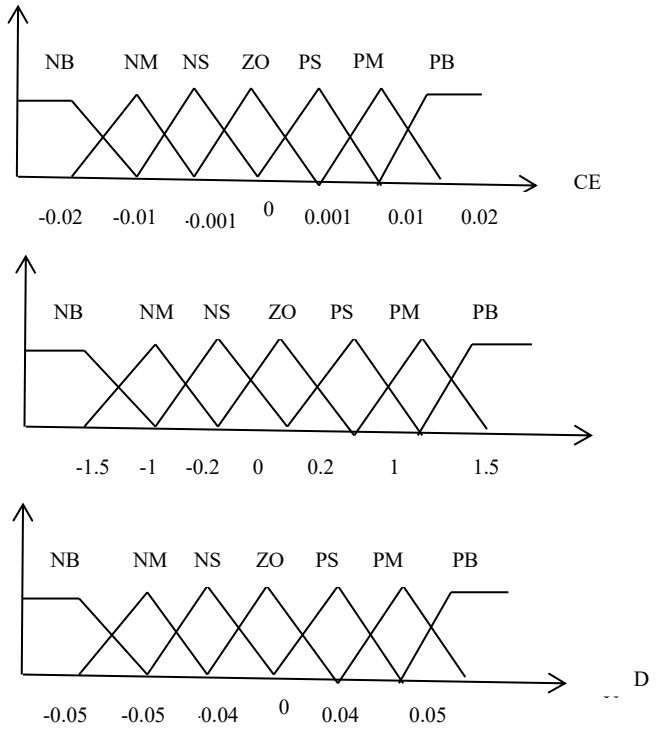

Fig.12. Membership function for the E, CE and DU

The Table 2. shows fuzzy rule base and factors of matrix is error (E), change error (CE) and duty ratio variation (dD).

Table 2 FLC rule base

E/ΔE	NB	NM	NS	ZO	PS	PM	PB
NB	NB	NB	NB	NB	NM	NS	ZO
NM	NB	NB	NM	NM	NS	ZO	PS
NS	NB	NM	NS	NS	ZO	PS	PM
ZO	NB	NM	NS	ZO	PS	PM	PB
PS	NM	NS	ZO	PS	PS	PM	PB

PM	NS	ZO	PS	PM	PM	PB	PB
PB	ZO	PS	PM	PB	PB	PB	PB

2.7 Design of ANFIS controller

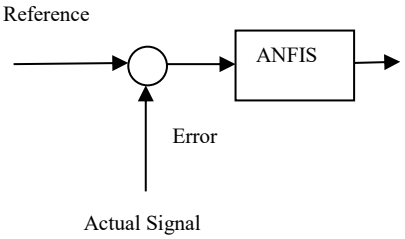

Fig.13. Design of ANFIS controller

The PI controllers are replaced by ANFIS controller and a typical control diagram is shown in Fig.13. Fuzzy Logic tool box in MATLAB has been used for designing and testing of the ANFIS controllers. The major steps are as follows.
The data required for training and testing the ANFIS are generated by designing and testing PI controllers for a set of different operating conditions.

Operation at different solar irradiation conditions.
After loading the data, the ANFIS structure gets generated by using grid partitioning method. For input and output, the Triangular and linear type membership functions have been considered in this work, respectively. For Sugeno-type ANFIS, a typical ANFIS structure obtained is shown in Fig.14.

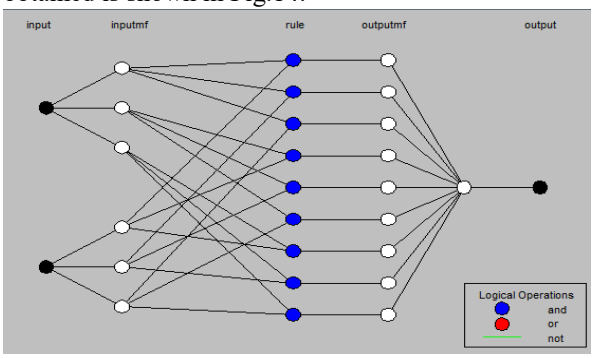

Fig.14. ANFIS model structure

3 Three phase inverter

Assume that three-phase grid voltage is symmetrical, stable and internal resistance is Zero; three phase loop resistance R_s and L_s are of the same value respectively; switching loss and on-state voltage is neglectable; affection of distribution parameter is neglectable; switching frequency of the rectifier is high enough [28].

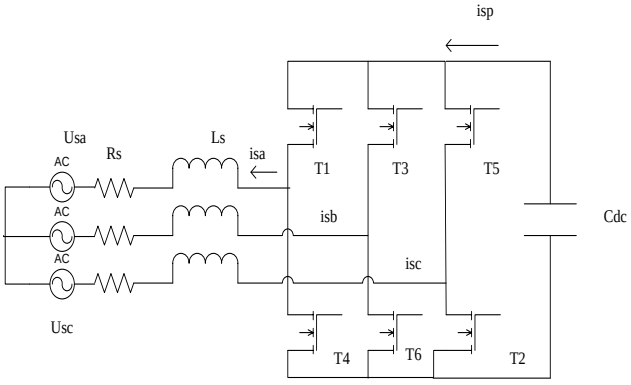

Fig.15. Three phase grid connected photovoltaic inverter

Basic operation principle of the inverter is to keep the dc-link voltage V_{dc} at a reference value V_{dc}* meanwhile keep the frequency and phase of output current are same as grid voltage. The error signal generated from voltage comparison is adjusteby voltage adjuster and it decides voltage adjuster and it decides the value of reference current, then it's used to switch ON and OFF the values of the inverter. The load of the grid-connected inverter is power grid, grid power is controlled by grid current [37].
The parameters are listed below.

I	output current of photovoltaic array
C_{dc}	Capacitance of the dc link
V_{dc}	DC link voltage
V_a, V_b, V_c	Voltage between leg midpoint and O point
V_{sa}, V_{sb}, V_{sc}	AC grid voltage
i_{sa}, i_{sb}, i_{sc}	AC grid current
L_s	Equivalent inductance of loop
R_s	Equivalent resistance of loop

Switching function S_k is defined as

$$S_k=\begin{cases}1 & \text{Up switch conducts lower switch blocks}\\ 0 & \text{Up switch conducts lower switch blocks}\end{cases} \quad (4)$$

Where k=a, b, c

According to Kirchhoff's law it can derive

$$\begin{cases} V_{sa} = -R_s i_{sa} - L_s p i_{sa} + S_a V_{dc} + V_{NO} \\ V_{sb} = -R_s i_{sb} - L_s p i_{sb} + S_b V_{dc} + V_{NO} \\ V_{sc} = -R_s i_{sc} - L_s p i_{sc} + S_c V_{dc} + V_{NO} \end{cases} \quad (5)$$

And

$$C_{dc}.\, p.\, V_{dc} + S_a i_{sa} + S_b i_{sb} + S_c i_{sc} = I \quad (6)$$

In three phase symmetrical system without neutral line

$$\begin{cases} V_{sa} + V_{sb} + V_{sc} = 0 \\ i_{sa} + i_{sb} + i_{sc} + 0 \end{cases} \quad (7)$$

Combine (5), (6) and (7) it can derive mathematical model of a three phase grid connected photovoltaic inverter in three phase (a, b, c) stationary reference frame.

$$\begin{cases} V_{sa} = -R_s i_{sa} - L_s p i_{sa} + S_a V_{dc} - \frac{S_a + S_b + S_c}{3} V_{dc} \\ V_{sb} = -R_s i_{sb} - L_s p i_{sb} + S_b V_{dc} - \frac{S_a + S_b + S_c}{3} V_{dc} \\ V_{sc} = -R_s i_{sc} - L_s p i_{sc} + S_c V_{dc} + V_{NO} \end{cases} \quad (8)$$

Expressed in matrix (8) can be written as

$$Y_p X = AX + u \quad (9)$$

While

$$Y = \begin{bmatrix} L_s & 0 & 0 & 0 \\ 0 & L_s & 0 & 0 \\ 0 & 0 & L_s & 0 \\ 0 & 0 & 0 & L_s \end{bmatrix} \quad (10)$$

$$p = \frac{d}{dt} \quad (11)$$

$$X = [-i_{sa}, -i_{sb}, -i_{sc}\, V_{dc}]^T \quad (12)$$

$$A = \begin{bmatrix} -R_s & 0 & 0 & -\left(S_a - \frac{S_a + S_b + S_c}{3}\right) \\ 0 & -R_s & 0 & -\left(S_a - \frac{S_a + S_b + S_c}{3}\right) \\ 0 & 0 & -R_S & -\left(S_a - \frac{S_a + S_b + S_c}{3}\right) \\ & & S_a \quad S_b \quad S_c & 0 \end{bmatrix} \quad (13)$$

$$u = \left[V_{sa,} V_{sb}, V_{sc}, I\right]^T \tag{14}$$

When switching frequency is much higher than grid voltage frequency, switching function S_k in can be substituted by duty cycle d_k (k=a, b, c), thus it can derive

$$A = \begin{bmatrix} -R_s & 0 & 0 & -\left(d_a - \frac{d_a+d_b+d_c}{3}\right) \\ 0 & -R_s & 0 & -\left(d_a - \frac{d_a+d_b+d_c}{3}\right) \\ 0 & 0 & -R_S & -\left(d_a - \frac{d_a+d_b+d_c}{3}\right) \\ & & S_a \quad S_b \quad S_c & 0 \end{bmatrix} \tag{15}$$

Adopting frame transformation, it can derive mathematical model in two-phase (α-β) stationary reference frame. The transforming matrix is

$$T_{\alpha\beta/abc} = \frac{2}{3}\begin{bmatrix} 1 & -\frac{1}{2} & -\frac{1}{2} \\ 0 & \frac{\sqrt{3}}{2} & -\frac{\sqrt{3}}{2} \end{bmatrix} \tag{16}$$

Adopt PARK transformation, it can derive mathematical model in two phase (d-q) rotating reference frame. The following matrix is

$$T_{dq/\alpha\beta} = \frac{2}{3}\begin{bmatrix} \cos\omega t & \sin\omega t \\ -\sin\omega t & \cos\omega t \end{bmatrix} \tag{17}$$

Transform (9) by (16) and (17), mathematical model of three phase photovoltaic inverter in d-q reference frame can be expressed as

$$\begin{cases} L_s p\,\overrightarrow{I_s^e} + j\omega L\,\overrightarrow{I_s^e} + R_s\overrightarrow{I_s^e} = \overrightarrow{V_r^e} - \overrightarrow{V_s^e} \\ C_d p V_{dc} = \overrightarrow{-D^e I_s^e} + I \end{cases} \tag{18}$$

While "e" represents that variables are in rotating reference frame. From (18)

$$[V_{sd} \quad V_{sq}]^T = T_{dq/\alpha\beta}.\,T_{\alpha\beta/abc}[V_{sa} \quad V_{sb} \quad V_{sc}]^T \tag{19}$$

$$[I_{sd} \quad I_{sq}]^T = T_{dq/\alpha\beta}.\,T_{\alpha\beta/abc}[i_{sa} \quad i_{sb} \quad i_{sc}]^T \tag{20}$$

$$[d_d \quad d_q]^T = T_{dq/\alpha\beta}.\,T_{\alpha\beta/abc}[d_a \quad d_b \quad d_c]^T \tag{21}$$

Grid voltage space vector $\overrightarrow{V_s^e}$ can be expressed as

$$\overrightarrow{V_s^e} = V_{sd} + jV_{sq} \tag{22}$$

Output grid current $\vec{I}_s^e$ can be expressed as

$$\vec{I}_s^e = i_{sd} + ji_{sq} \tag{23}$$

Switching function vector $\vec{D}^e$ can be expressed as

$$\vec{D}^e = d_d + jd_q \tag{24}$$

Neutral voltage vector of converter leg midpoint can be expressed as

$$\vec{V}_r^e = \vec{D}^e . V_{dc} = V_{dc}(d_d + jd_q) = V_{rd} + jV_{rq} \tag{25}$$

4 Synchronous PI current control

This paper adopts synchronous PI current control strategy in two-phase rotating (d-q) frame, current loop achieves sinusoidal control of inverter, and according to synchronous rotating frame control structure, three-phase symmetric grid voltage and grid current becomes DC variables, so adopting PI controller, current loop can be realize no steady-state error adjustment. Grid voltage can be expressed as [29]

$$\begin{cases} V_{sa} = V_m \sin\omega t \\ V_{sb} = V_m \sin(\omega t - \frac{2\Pi}{3}) \\ V_{sc} = V_m \sin(\omega t + \frac{2\Pi}{3}) \end{cases} \tag{26}$$

Adopt $T_{\alpha\beta/abc}$ and $T_{dq/\alpha\beta}$ transformation, it drives

$$\begin{bmatrix} V_{sd} \\ V_{sq} \end{bmatrix} = \begin{bmatrix} \cos\omega t & \sin\omega t \\ -\sin\omega t & \cos\omega t \end{bmatrix} \frac{2}{3} \begin{bmatrix} -1 & -\frac{1}{2} & -\frac{1}{2} \\ 0 & \frac{\sqrt{3}}{2} & -\frac{\sqrt{3}}{2} \end{bmatrix} \begin{bmatrix} V_{sa} \\ V_{sb} \\ V_{sc} \end{bmatrix} = \begin{bmatrix} V_m \\ 0 \end{bmatrix} \tag{27}$$

From (31), in synchronous rotating frame, V_{sd} and V_{sq} are DC variable, thus it can adopt two PI adjusters to control realizing tracking of reference current. Substitute (27) in (18), and ignore R_s, it drives

$$\begin{cases} L_s \frac{di_{sd}}{dt} - \omega L_s i_{sq} = V_{rd} - V_m \\ L_s \frac{di_{sq}}{dt} - \omega L_s i_{sd} = V_{rq} \end{cases} \tag{28}$$

Mathematical model of (28) shows that it's strong coupling system. In order to eliminate the interference between d and q axis, it adopts decoupled control.

$$V_{rd} = V_{m-}\omega L_s i_{sq} + V_{id}$$
$$V_{rq} = \omega L_s i_{sd} + V_{iq} \quad (29)$$

V_{id} and V_{iq} are outputs of d, q axis PI adjusters

$$V_{id} = k_p(i^*_{sd} - i_{sd}) + k_i \int (i^*_{sd} - i_{sd})dt$$
$$V_{iq} = k_p(i^*_{sq} - i_{sq}) + k_i \int \left(i^*_{sq} - i_{sq}\right)dt \quad (30)$$

Substitute (29) and (30) into (28), it drives

$$L_s \frac{di_{sd}}{dt} = k_p(i^*_{sd} - i_{sd}) + k_i \int (i^*_{sd} - i_{sd})dt$$

$$L_s \frac{di_{sq}}{dt} = k_p(i^*_{sq} - i_{sq}) + k_i \int \left(i^*_{sq} - i_{sq}\right)dt \quad (31)$$

5 Power losses and junction temperature analysis of semiconductor devices

As with the increased application and usage of semi-conductor devices, the estimation of the power loss and temperature of the junction and thermal model (case and sink) has become a major issue with the increase of the capacity and switching frequency of devices. One method for estimation of power loss of devices is based on the exact current and voltage waveforms of the devices. But, it is very difficult to get the waveforms from simulating each pulse of PWM exactly, with the variation of current and voltage. Usually the power loss is calculated under the constant junction temperature. However, the power loss does depend on the junction temperature, not only the loss of saturation, but also the loss of transient switching operation. Therefore, the power loss estimation and the junction temperature calculation should be combined to find out the working point of devices [38]. The power loss of each switching operation of semiconductor device (IGBT) is divided into three main portions, which are illustrated in Fig. 8. Total power loss during each pulse of the IGBT is the sum of turn-on loss, turn-off loss, and saturation loss. Also, the losses of the anti-paralleled diode are included, if any.

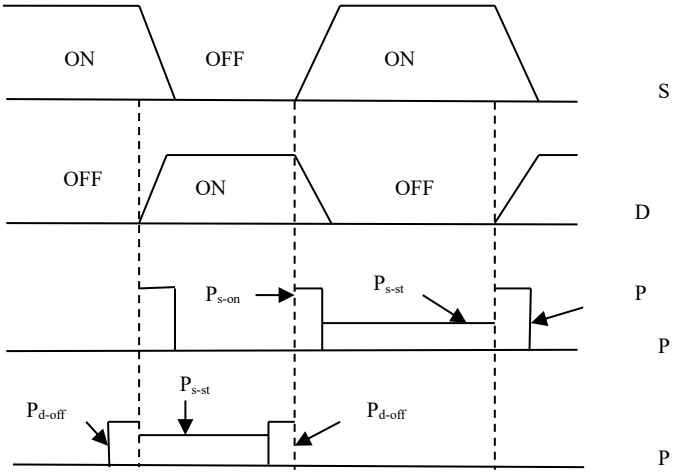

Fig.16. Power loss estimation

It can be assumed that the IGBT power loss of turn-on or turn-off depends on the dc-link voltage and collector current of the IGBT. From application, it was found that the transient switching waveforms change with increase of junction temperature (6). It should be pointed out that the turn-on loss and turn-off loss are also functions of junction temperature which are expressed in (32), (33), (35) and (36). The saturation voltage of the IGBT and its antiparallel diode is usually defined as the function of junction temperature and collector current which are shown in (33) and (37).

$$P_{s-on} = f_{s-on}(V_d, i, T_j) \quad (32)$$

$$P_{s-off} = f_{s-off}(V_d, i, T_j) \quad (33)$$

$$V_{s-st} = f_{s-st}(i, T_j) \quad (34)$$

$$P_{d-on} = f_{d-on}(V_d, i, T_j) \quad (35)$$

$$P_{d-off} = f_{d-off}(V_d, i, T_j) \quad (36)$$

$$V_{d-st} = f_{d-st}(i, T_j) \quad (37)$$

Where

$P_{s\text{-}on}$= Power Losses during on time of the IGBT
$P_{s\text{-}off}$= Power Losses during off time of the IGBT
$P_{d\text{-}on}$= Power Losses during on state of the Diode
$P_{d\text{-}off}$= reverses recovery losses of the Diode
$P_{d\text{-}off}$= reverses recovery losses of the Diode

6 Thermal model

A state-space block is used to build a one-cell Cauer network modeling the thermal capacitance of the device junction as well as its junction-to-case thermal resistance. The state space equations are given below:

$$x' = \left[\frac{-1}{R_{th}C_{th}}\right] x + \left[\frac{1}{R_{th}C_{th}} \quad \frac{1}{C_{th}}\right] \begin{bmatrix} T_c \\ P_l \end{bmatrix} \tag{38}$$

$$\begin{bmatrix} T_j \\ P_c \end{bmatrix} = \begin{bmatrix} 1 \\ \frac{1}{R_{th}} \end{bmatrix} x + \begin{bmatrix} 0 & 0 \\ \frac{-1}{R_{th}} & 0 \end{bmatrix} \begin{bmatrix} T_c \\ P_l \end{bmatrix} \tag{39}$$

where, T_j is junction temp of IGBT, P_l is power loss across IGBT, T_c is case temperature of IGBT, R_{th} is junction to case thermal resistance. C_{th} is thermal capacitance of junction; P_c is heat flow from junction to case. Now by calculating the junction temperature we can calculate the power losses of the IGBT. The same analysis is extended for power losses and junction temperature calculation of anti-parallel diode.

7 Result and discussion

The schematic diagram of the main system of 100.7 kW is shown in Fig.1. The modeling and simulation has been done using Matlab/Simulink software. The main system parameters are given in Table 3. The system is simulated with zero initial conditions hence results are settling down to steady-state values after transient period. The MPPT algorithms have been activated at the 0.4 s instant.

Table3 System Parameters

T_{pv}	Temperature of PV cells	25^0C
G	Irradiance of PV cells	1kW/m^2

The SPV array has been simulated and the steady state voltage output is 240V and the boost converter has been used to boost the voltage level at steady-state without MPPT as shown in Fig. 17. The operating voltage of the SPV array increases after using MPPT algorithms (MPPT algorithm starts at 0.4s). The grid current follows the sinusoidal waveform as shown in Fig. 18 and the Total Harmonic Distortion (THD) is 2.85% which is acceptable as per the IEEE-519 standard.

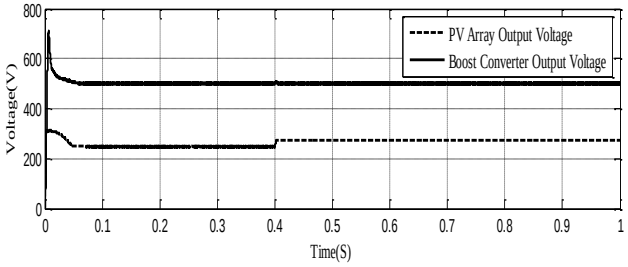

Fig.17. DC output voltage of PV array and DC-DC boost converter

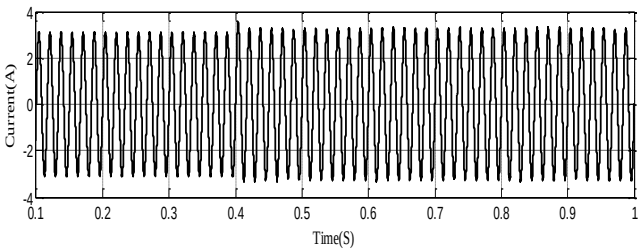

Fig.18. Grid current

The switching losses of the DC-DC boost converter are higher in absence of MPPT algorithms as shown in Fig.21. The switching losses are less using MPPT and losses are less using ANFIS controller as compared to FLC. The energy injected into the grid using ANFIS controller is better than FLC controller and the efficiency of the SPV system is 99.11% using ANFIS controller as compared to FLC controller having efficiency of 99.06%. The Fig. 19 clearly show the advantage of using controllers, as energy injected into the grid has increased from 95.6 kW to almost 100.7 kW after the instant 0.4s when MPPT algorithm activated.

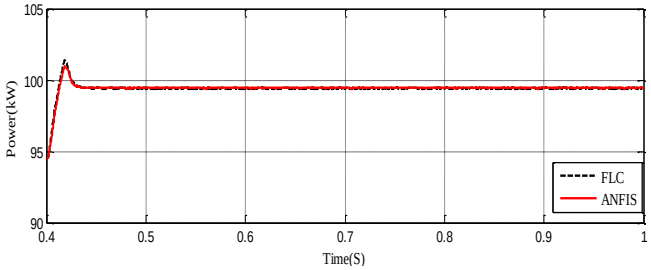

Fig.19. Comparison of energy injected into the grid

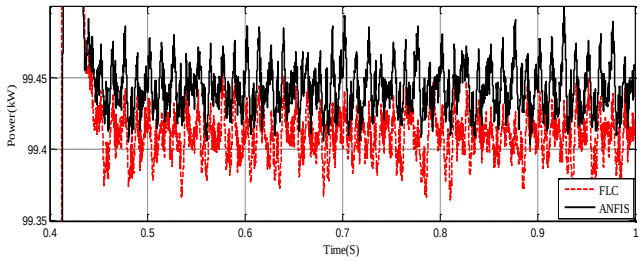

Fig.20. Comparison of energy injected into the grid with closer look

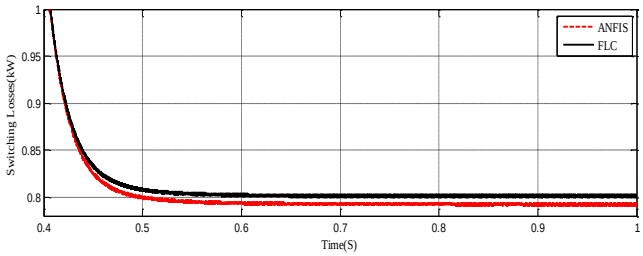

Fig.21. Comparison of switching losses of boost converter

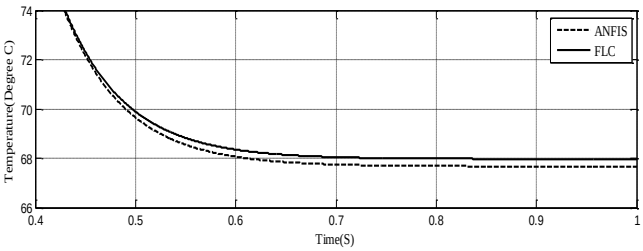

Fig.22. Comparison of sink temperature of IGBT and diode

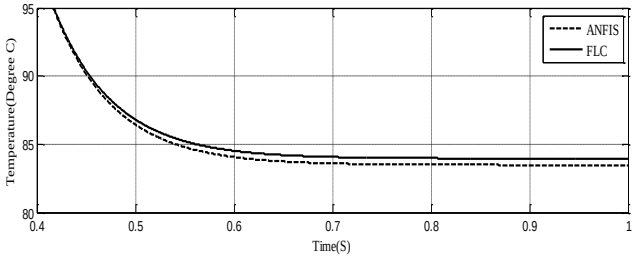

Fig.23. Comparison of case temperature of IGBT and diode

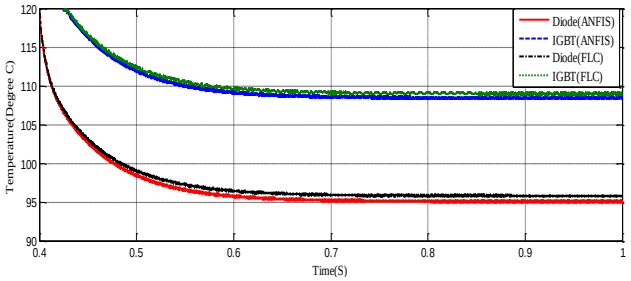

Fig.24. Comparison of junction temperature of IGBT and diode

References

1. J. Li, H. Wang.:Jones, L.,'A noval stand alone PV generation system based on variable step size INC MPPT and SVPWM control'. Power Electronics and Motion Control Conference on POWER AND ENERGY SYSTEMS, 2009.
2. J. J. Schoeman, J. D. van Wyk.,'A simplified maximal power controller for terrestrial photovoltaic panel arrays'. 13th Annu. IEEE Power electronics Spec. Conference, 1982, pp.361–367.
3. M. Buresch.: ' Photovoltaic Energy Systems'(New York: McGraw Hill, 1983)
4. G. W. Hart, H. M. Branz, C. H. Cox., 'Experimental tests of open loop maximum-power-point tracking techniques ' Solar Cells 1984, pp.185–195
5. D. J. Patterson.,'Electrical system design for a solar powered vehicle' 21st Annu. IEEE Power electronics Conference, 1990, pp.618–622
6. M. A. S. Masoum, H. Dehbonei, E. F. Fuchs.,'Theoretical and experimental analysis of photovoltaic systems with voltage and current based maximum power point tracking' IEEE Trans. Energy Convers., 2002, Vol:17, pp.514-522
7. H.-J. Noh, D.-Y. Lee, D.-S. Hyun., 'An improved MPPT converter with current compensation method for small scaled PV-applications' Annu. Conf. Ind. Electron. Soc., 2002, pp.1113–1118.
8. K. Kobayashi, H. Matsuo, Y. Sekine.,'A novel optimum operating point tracker of the solar cell power supply system' IEEE Power Electron. Spec. Conference, 2004, pp.2147–2151.
9. B. Bekker, H. J. Beukes.,'Finding an optimal PV panel maximum power point tracking method' 7th AFRICON Conf. Africa ,2004, pp.1125–1129.
10. T. Noguchi, S. Togashi, R. Nakamoto.:'Short-current pulse based adaptive maximum-power-point tracking for photovoltaic power generation system' IEEE Int. Symp. On Ind. Electron, 2000, pp.157–162.
11. N. Mutoh, T. Matuo, K. Okada, M. Sakai.,'Prediction-data-based maxi mum-power-point-tracking method for photovoltaic power generation systems' IEEE Power electronics Spec. Conference, 2002, pp.1489–1494.
12. S. Yuvarajan, S. Xu., 'Photo-voltaic power converter with a simple maximum-power-point-tracker' Int. Symp. Circuits System, 2003, pp.399–402.
13. B. M.Wilamowski, X. Li.,'Fuzzy system based maximum power point tracking for PV system' 28th Annu. Conf. IEEE Ind. Electron, 2002, pp.3280–3284.
14. M. Veerachary, T. Senjyu, K. Uezato.,'Neural-network-based maximum-power-point tracking of coupled-inductor interleaved-boost converter-supplied PV system using fuzzy controller'IEEE Trans. Ind. Electronics, vol: 50, pp.749–758.
15. M. Veerachary, T. Senjyu, K. Uezato, Neural-network-based maximum-power-point tracking of coupled-inductor interleaved-boost converter-supplied PV system using fuzzy controller, IEEE Trans. Ind. Electronics, vol. 50, 2003, pp.749–758.
16. N. Khaehintung, K. Pramotung, B. Tuvirat, P. Sirisuk., 'RISC microcontroller built-in fuzzy logic controller of maximum power point tracking for solar-powered light-flasher applications' 30th Annu. Conf. IEEE Ind. Electron. Soc., 2004, pp.2673–2678.
17. K. Ro, S. Rahma, Two-loop controller for maximizing performance of a grid-connected photovoltaic-fuel cell hybrid power plant, IEEE Trans. Energy Conversion, vol.13(3), 1998, pp.276-281.
18. A. Hussein, K.Hirasawa, J. Hu, J. Murata.,'The dynamic performance of photovoltaic supplied dc motor fed from DC–DC converter and controlled by neural networks' Int. Joint Conf. Neural Network, 2002, pp.607–612.
19. X. Sun, W. Wu, X. Li, Q. Zhao.,'A research on photovoltaic energy controlling system with maximum power point tracking. Power Convers. Conference, 2002, pp.822–826.

20. L. Zhang, Y. Bai, A. Al-Amoudi.,'GA-RBF neural network based maximum power point tracking for grid-connected photovoltaic system' Int. Conf. Power Electronics Machines and Drives, 2002, pp.18–23.
21. H. Afgoul, F. Krim.,'intelligent energy management in a photovoltaic installation using neuro-fuzzy technique' IEEE ENERGYCON Conference and Exhibition, 2012, pp. 20–25.
22. Fangrui Liu, Shanxu Duan, Fei Liu, Bangyin Liu, Yong Kang.,'A Variable Step Size INC MPPT for PV systems' IEEE Transaction on Industrial Electronics, vol. 55, 2008, pp. 2622 – 2628.
23. Ciobotaru, M. kerekes, T. Teodorescu., 'PV inverter simulation using MATLAB/SIMULINK graphical environment' IEEE Industrial Electronics IECON, pp. 5313 – 5318.
24. R. V. Dell' Aquila, L. Baboni, R. Morici.,'A new approach: modeling simulation, development and implementation of a commercial grid-connected transformerless PV inverter' International Symposium on Power Electronics, Electrical Drives, automation and Motion, 2010.
25. O. Wasynezuk.,'Dynamic behavior of a class of photovoltaic power systems' IEEE Transactions on Power Apparatus and Systems, pp. 3031-3037, September 1983.
26. J.-S. Jang, 'ANFIS: adaptive-network-based fuzzy inference system' IEEE Transactions on Systems, Man and Cybernetics, vol. 23, no.3, pp. 665-685, May 1993
27. S.-J. Kang, J.-S. KO, J.-S. Choi, M.-G. Jang, J.-H. Mun, J.-G. Lee, and D.-H. Chung., 'A Novel MPPT Control of photovoltaic system using FLC algorithm' in 11th International Conference on Control, Automation and Systems (ICCAS), 2011, pp. 434-439.
28. Liang Ma., 'Nonlinear PID control for three phase PWM rectifier based on predictive current control' ICIEA, 2008, pp. 649-653.
29. Liang. Ma, Wang Ran, Trillion Q. Zheng., 'Modeling and control of 100kW three-pahse grid connected photovoltaic inverter'5th IEEE Conference on Industrial Electronics and Applications, 2010.
30. D. Xu, H. Lu, L. Hung Liu, Satoshi, S. Azuma., 'Power Loss and Junction Temperature Analysis of Power Semiconductor Devices' IEEE Transaction on Industry Applications, vol. 38, 2010, pp. 1426 – 1431.